Cytoplasmic Irradiation Induces Metabolic Shift in Human Small Airway Epithelial Cells via Activation of Pim-1 Kinase

Authors: Wu, Jinhua, Zhang, Qin, Wuu, Yen-Ruh, Zou, Sirui, and Hei, Tom K.

Source: Radiation Research, 187(4) : 451-463

Published By: Radiation Research Society

URL: https://doi.org/10.1667/RR0006CC.1

RADIATION RESEARCH **187**, 451–463 (2017)
0033-7587/17 $15.00

DOI: 10.1667/RR0006CC.1

Cytoplasmic Irradiation Induces Metabolic Shift in Human Small Airway Epithelial Cells via Activation of Pim-1 Kinase

Jinhua Wu,[a,d] Qin Zhang,[c] Yen-Ruh Wuu,[a] Sirui Zou[a] and Tom K. Hei[a,b,1]

[a] *Center for Radiological Research, College of Physicians and Surgeons; Columbia University, New York, New York 10032;* [b] *Department of Environmental Health Sciences, Mailman School of Public Health, Columbia University, New York, New York 10032;* [c] *Department of Environmental Health and Occupational Medicine, West China School of Public Health, Sichuan University. Chengdu, Sichuan, China 610041; and* [d] *Institute of Plasma Physics, Chinese Academy of Sciences, Hefei, Anhui, China 230031*

Wu, J., Zhang, Q., Wuu, Y., Zou, S. and Hei, T. K. Cytoplasmic Irradiation Induces Metabolic Shift in Human Small Airway Epithelial Cells via Activation of Pim-1 Kinase. *Radiat. Res.* 187, 451–463 (2017).

The unique cellular and molecular consequences of cytoplasmic damage caused by ionizing radiation were studied using a precision microbeam irradiator. Our results indicated that targeted cytoplasmic irradiation induced metabolic shift from an oxidative to glycolytic phenotype in human small airway epithelial cells (SAE). At 24 h postirradiation, there was an increase in the mRNA expression level of key glycolytic enzymes as well as lactate secretion in SAE cells. Using RNA-sequencing analysis to compare genes that were responsive to cytoplasmic versus nuclear irradiation, we found a glycolysis related gene, Pim-1, was significantly upregulated only in cytoplasmic irradiated SAE cells. Inhibition of Pim-1 activity using the selective pharmaceutic inhibitor Smi-4a significantly reduced the level of lactate production and glucose uptake after cytoplasmic irradiation. In addition, Pim-1 also inhibited AMPK activity, which is a well-characterized negative regulator of glycolysis. Distinct from the glycolysis induced by cytoplasmic irradiation, targeted nuclear irradiation also induced a transient and minimal increase in glycolysis that correlated with increased expression of Hif-1α. In an effort to explore the underline mechanism, we found that inhibition of mitochondria fission using the cell-permeable inhibitor mdivi-1 suppressed the induction of Pim-1, thus confirming Pim-1 upregulation as a downstream effect of mitochondrial dysfunction. Our data show and, for the first time, that cytoplasmic irradiation mediate expression level of Pim-1, which lead to glycolytic shift in SAE cells. Additionally, since glycolysis is frequently linked to cancer cell metabolism, our findings further suggest a role of cytoplasmic damage in promoting neoplastic changes.

INTRODUCTION

Development of modern, sophisticated microbeam facilities with precise dose delivery system allows one to study radiation response within subcellular range using *in vitro* cell models. By carefully selecting subcellular targets, we examined the role of both the cytoplasm and nucleus in responding to α-particle radiation. Our studies have shown that extranuclear targets play important roles in ionizing radiation mediated genotoxic effects and mutagenesis (*1–4*). Contrary to the cell damaging effect of targeted nuclear irradiation, we found that cytoplasmic irradiation is mutagenic while inflicting minimal cytotoxicity (*3*). Targeted cytoplasmic irradiation induces oxidative DNA damage and reactive oxygen and nitrogen species (ROS and RNS), which then leads to an increase in cyclooxygenase-2 (COX-2) expression and activation of extracellular signal-related kinase (ERK) pathways (*1*). Recently we reported the important role of mitochondria-dependent signaling in radiation-induced bystander effects (*5*) as well as in targeted cytoplasmic irradiation (*2*). Levels of the mitochondrial fission protein, dynamin-related protein 1 (DRP1) has been shown to be increased in cytoplasmic-irradiated cells and demonstrated to be the causal link between cytoplasmic irradiation and mitochondrial fission and dysfunction (*2*). In the current study we further examined the metabolic changes in human small airway epithelial (SAE) cells after cytoplasmic irradiation. We found upregulations of key glycolytic genes shortly after cytoplasmic irradiation and reported our novel finding of Pim-1 as the regulator of glycolysis after cytoplasmic irradiation. Our findings suggested a unique role of cytoplasmic irradiation which can be targeted in environmental toxicity studies and radiation therapy.

In nontransformed cells, steady-state aerobic glycolysis is generally low without exogenous growth stimuli or environmental stress. However, malignant cells are metabolically transformed to sustain a high-basal glycolytic rate (*6–8*). Hyperactive glycolysis provides quick supply of ATP as well as a primary route for carbon influx, which is required for biosynthesis of essential macromolecules and

[1] Address for correspondence: Center for Radiological Research, College of Physicians and Surgeons; Columbia University, 630 West 168th Street, VC 11-205, New York, New York 10032, email: tkh1@cumc.columbia.edu.

formation of organelles in aggressively proliferating cells (*6–8*). There is substantial evidence that in cancer cells glycolysis is driven by overexpression or hyperactivity of key glycolytic enzymes, most of which are downstream targets of activated oncogene and/or inactivated tumor suppressors (*9, 10*). Furthermore, mutations of mitochondrial DNA that impair respiratory complex functions also leads to high glycolytic rate (*11*). Although targeted cytoplasmic irradiation has been shown to alter the dynamic equilibrium of mitochondrial fission and fusion, its effects on cellular metabolism, particularly on cellular glycolysis is not known. It remains to be determined whether radiation-induced damage of mitochondria could result in metabolic changes as a result of increased ROS.

Pim-1 belongs to a group of constitutively activated serine/threonine kinases (*12*). The three members in the Pim family, PIM1 (chromosome 6), PIM2 (chromosome X) and PIM3 (chromosome 22), are implicated in the growth and progression of hematological malignancies (*13*), prostate cancer (*14*) and gastric cancer (*15*). Pim-1 has been shown to cooperate with c-Myc to induce prostate cancer (*16*) through transcriptional upregulation of its expression (*17*) and stabilization of its protein (*18*). Studies exploring the function of Pim kinases reported that Pim-1 directly phosphorylates Cdc25C (*19*), Pim-2 regulates p27Kip1 (*20*) and Pim-3 phosphorylates and inhibits BAD (*21*). It is likely that these enzymes play a role in cell cycle progression and anti-apoptosis. Pim kinases have also been demonstrated to promote the activation of the rapamycin-sensitive mammalian target of rapamycin (mTORC1) (*22*) and inhibit adenosine monophosphate-activated protein kinase (AMPK) (*23*). AMPK senses the cellular energy status and becomes activated when cellular ATP levels decline with concomitant rise in AMP levels (*24*). Activated AMPK down-regulates the energetically demanding process of protein synthesis (*24*) and functions as a negative regulator of glycolysis (*25*).

The mechanism of ionizing radiation-induced glycolysis have been studied recently, primarily focused on the increased transcriptional activity of hypoxia inducible factor-1 alpha (HIF-1α) under normoxic condition (*26*). Little is known about the interim process between mitochondrial stress induced by ROS and the induction of cellular glycolytic phenotype. In the current study, we compared different gene expression patterns in SAE cells after irradiation through either the cytoplasm or nucleus. Consistent with other report, we found HIF-1α induction in nuclear irradiated cells. However, in cytoplasmic irradiated cells, no increase in HIF-1α was detected even though a transcriptional increase in glycolytic enzymes including hexokinase 2 (HK2), glucose transporter 3 (GLUT3) and Peroxisome Proliferator-Activated Receptor Gamma Coactivator 1 alpha (PGC-1α) was found. Instead, a rapid and sustained increase of Pim-1 was observed after cytoplasmic irradiation. Using Smi-4a, the selective pharmaceutic inhibitor of Pim-1, and CRISPR/Cas9 knockdown of Pim-1, our results confirmed the important role of Pim-1 in regulating glycolysis. Our novel results report the role of cytoplasmic irradiation in mediating cell metabolic shift and drew a causal link between Pim-1 and mitochondrial stress induced glycolysis.

MATERIALS AND METHODS

Materials

Anti-Pim-1, phospho-AMPKα (T172) antibodies were purchased from Cell Signaling (Danvers, MA). Dimethyl sulfoxide, propidium iodide, mdivi-1, and Smi-4a were purchased from Sigma (St. Louis, MO). Hif-1α inhibitor was purchased from EMD Millipore (Billerica, MA). 2-NBDG (2-(N-(7-Nitrobenz-2-oxa-1,3-diazol-4-yl)Amino)-2-Deoxyglucose) was purchased from ThermoFisher (Waltham, MA).

Cell Line and Culture

The human telomerase reverse transcriptase (hTERT) immortalized human SAE cells were previously generated (*27*). Cells were maintained in serum-free small airway epithelial cell growth medium supplemented with various growth factors supplied by the manufacturer (Lonza, Walkersville, MD). Cultured cells were maintained at 37°C in a humidified 5% CO_2 incubator.

Microbeam Irradiation

Microbeam irradiations were performed at Radiological Research Accelerator Facility (RARAF), Columbia University. Approximately 500 SAE cells were plated overnight on microbeam dishes coated with Cell-Tak (BD Biosciences, San Jose, CA) to enhance cell attachment. Immediately before irradiation, the culture medium was removed from the microbeam dishes and a moisture cover was placed over the objective lens to keep the cells from being dehydrated during the 15-min irradiation time. The microbeam image analysis system was used to visualize the nuclei stained with Hoechst 33342. For cytoplasmic irradiation, five 5.1 MeV 4He ions were delivered at two target positions, 8 μm away from each end of the cell nucleus along the major axis of the nucleus as described previously (*3*). For nuclear irradiation, five 5.1 MeV 4He ions were delivered to the center of nucleus. The particle fluency was measured by a detector positioned above the cells. After every cell on the plate had been irradiated, fresh medium was added and the dishes were kept in the incubator at 37°C until processed. All control cells were stained with Hoechst 33342 and sham irradiated. In selected experiments where endpoints at 2 weeks postirradiation were to be examined, cells were trypsinized and pooled from 3 original microbeam dishes at 24 h postirradiation and subcultured in T25 culture flasks until use.

RNA-Seq

SAE cells were selectively irradiated through either the nucleus or cytoplasm as described above. Cells were then incubated for 2 h before harvesting using Trizol (ThermoFisher, Waltham, MA). Fifty individual microbeam dishes for each treatment (control, CI and NI) were pooled into one 2 ml Trizol solution and RNA was extracted using the RNeasy Micro kit (Qiagen, Germantown, MD) following manufacturer's instruction with modification. In general, RNA was extracted to the aqueous layer by adding the same volume (2 ml) of 100% ethanol and centrifuging at 15,000 rpm for 15 min at 4 °C. The aqueous phase was then transferred into Qiagen MinElute spin column and followed manufacturer's protocol. Samples containing 100 ng RNA with RIN $>$ 9.5 were sent to Columbia University Genome Center for RNA-sequencing. Triplicate samples of each treatment were sequenced ($N = 3$). RNA-seq was proceed on library preparation by using Illumina TruSeq RNA prep kit. Libraries are then sequenced

TABLE 1
QPCR Primer Sequences

Name	Forward	Reverse
Pim-1	ACGACCTGCACGCCACCAAG	TCGGAGACGCGGATGCCTGA
HK2	CCCCGGCAAGCAGAGGTTCG	CGCTCTGAGATGCGGCCTCG
GLUT3	GTGGCCGGCTGCTCCAACTG	CCTGCCACGGGTCTCAGGGA
PGC-1α	ACAGCCGTCGGCCCAGGTAT	GCCTCTCCCTTTGCTTGGCCC
PKM2	CGGTGCAACCGAGCTGGGAA	GCATGCGCACAGCCTCCAGA

using Illumina HiSeq2000. Samples were multiplexed in each lane, which yields targeted number of single-end/paired-end 100 base pair reads for each sample, as a fraction of 180 million reads for the whole lane. RTA (Illumina) was used for base calling and bcl2fastq (version 1.8.4) for converting BCL to fastq format, coupled with adaptor trimming. The reads were mapped to a reference genome (Human: NCBI/build37.2) using Tophat (*28*) (version 2.0.4) with 4 mismatches (–read-mismatches = 4) and 10 maximum multiple hits (–max-multihits = 10). To tackle the mapping issue of reads that are from exon–exon junctions, Tophat infers novel exon–exon junctions *ab initio*, and combine them with junctions from known mRNA sequences (refgenes) as the reference annotation. The expression level of genes and splice isoforms were estimated using cufflinks (*29*) (version 2.0.2) with default settings. Differentially expressed genes were tested under various conditions using DEseq (*30*). It is an R package based on a negative binomial distribution that models the number reads from RNA-seq experiments and test for differential expression. Benjamini corrected P values <0.05 were considered significant. One hundred eleven and 97 genes were significant in cytoplasmic and nuclear irradiated samples compared to control, respectively. The significant genes are listed in Supplementary Materials (Table S1 and S2; http://dx.doi.org/10.1667.1.S1). Biological functions were determined using the significant genes with ToppGeneknowledgebase (https://toppgene.cchmc.org/enrichment.jsp), based on Gene Ontology (GO) gene annotations, Benjamini corrected P values <0.05 were considered significant.

Quantification of Real-Time PCR

After microbeam irradiation, cells were washed twice with cold PBS at 24 h or 2 weeks as indicated before mRNA was extracted using Trizol and converted to cDNA using High Capacity cDNA reverse transcription kit (ThermoFisher Scientific, Waltham, MA). The QPCR probe sequences are listed in Table 1. Gene expressions were measured by Life Technologies ViiA 7 Real Time PCR System in standard mode using SYBR Green QPCR mix (ThermoFisher Scientific, Waltham, MA). Triplicate samples were used for control, CI and NI at two different time point. Data were analyzed using the delta delta CT method.

Immunofluorescence

After microbeam irradiation, cells were washed twice with cold phosphate buffered saline (PBS) at indicated time points, fixed with 4% paraformaldehyde in PBS for 20 min at room temperature, and subsequently washed twice with PBS. Cells were then permeabilized with 0.2% Triton X-100 in PBS for 15 min, washed twice with PBS, and stained with specific antibodies, in combination with Alexa Fluor 488 goat anti-rabbit IgG secondary antibody. Propidium iodide (Sigma, St. Louis, MO) was used to visualize nuclei and fluorescent images were captured using a Nikon confocal microscope. Pim-1 inhibitor Smi-4a or Hif-1α inhibitor was added 30 min before irradiation and added back to culture medium after irradiation for indicated time.

Fluorescent Density Measurement

Cellular fluorescent density was measured using ImageJ software. Cells were selected using drawing/selecting tools. Selected area, integrated density and mean gray value were obtained. Background values were obtained from background area directly next to the cell of interest. Corrected total cell fluorescence was calculated using the equation CTCF = Integrated Density – (Area of selected cell * Mean fluorescence of background readings). Triplicate samples (N = 3) were used for each treatment. At least 5 images were taken from each repeat and 100 random cells were chosen to be quantified from the 5 images.

2-[N-(7-nitrobenz-2-oxa-1,3-diazol-4-yl) amino]-2-deoxy-d-glucose (2-NBDG) Uptake Assay

Five hundred SAE cells were plated onto microbeam dishes and irradiated through cytoplasm, nucleus or sham irradiated as described above. Cells were incubated for 24 h postirradiation with 50 μ*M* 2-NBDG was added to the dishes for the last 1 h. The 2-NBDG uptake reaction was stopped by removing the incubation medium and washing the cells twice with pre-cold PBS. Cells were then fixed with 4% paraformaldehyde in PBS for confocal microscopy imaging or trypsinized and re-suspended for flow cytometry. For the 2-week-treatment-time point, irradiated cells were trypsinized and pooled from 3 dishes for each treatment group (control, CI and NI). Cells were allowed to proliferate for 2 weeks before 20,000 cells were plated into 6-well plates and allowed to reach 50% confluency. The 2-NBDG at final concentration of 50 μ*M* was added to culture medium and incubated for 1 h. The cells were then washed twice with pre-cold PBS and fixed with 4% paraformaldehyde in PBS for confocal microscopy imaging.

Flow Cytometry Analysis

After incubation with 2-NBDG for 1 h, cells were re-suspended in 1 ml pre-cold PBS and then Propidium Iodide was added to a final concentration of 1 μg/ml. Cells were maintained at 4°C for flow cytometry analysis performed within 30 min. For each measurement, data from 10,000 single cell events was collected using a FACScalibur (Becton Dickinson) flow cytometer.

Lactate Production Assay

Lactate levels were measured using a colorimetric assay (Eton Bioscience, San Diego, CA) based on the lactate oxidase reaction, according to the manufacturer's protocol. The lactate concentrations were normalized per million cells.

Generation of CRISPR/Cas9-Mediated Pim-1 Knockdown Cells

Six guide RNAs (gRNAs) targeting Pim-1 were designed and inserted into lentiCRISPRv2 vector. Lenti-virus were generated using 293FT cells. SAE cells were infected with lenti-virus for 48 h before the homogeneity of Pim-1 knockdown was achieved by puromycin selection, followed by a complete medium change. gRNA targeted sequences are listed in Table 2.

Western Blotting

Cells were lysed using RIPA buffer. Protein concentrations were measured using Bradford protein assay kit (Bio-Rad, Hercules, CA) according to the manufacturer's protocol. Total cellular proteins were

TABLE 2
gRNA Sequence for Pim-1

gRNA-1	GGCCCGCTACTGGGCAGCGG
gRNA-2	GGCTTCGGCTCGGTCTACTC
gRNA-3	CCGCGTCTCCGACAACTTGC
gRNA-4	AGAAGGACCGGATTTCCGAC
gRNA-5	TAATGGCACTCGAGTGCCCA
gRNA-6	GGAAGTGGTCCTGCTGAAGA

resolved by SDS-PAGE, transferred to immunoblot membrane (polyvinylidene difluoride, Millipore, Billerica, MA) and immunoblotted with antibodies following the protocols of manufacturers. Immunocomplexes were visualized with SuperSignal Chemiluminescent HRP Substrates (ThermoFisher Scientific, Waltham, MA).

Statistical Analysis

Data were presented in the format mean ± SD, representative of three independent experiments. Statistical analyses were performed using the Student *t* test. $P < 0.05$ was considered to be statistically significant between the sham-irradiated control and targeted irradiation groups. In all figures, the statistical significances were indicated with $*P < 0.05$ or $**P < 0.01$.

RESULTS

RNA Sequencing Results Suggested Distinct Function of Cytoplasmic Irradiation

There is evidence that radiation that targets either nucleus or cytoplasm resulted in different biological responses in mammalian cells (*3*). In the current studies, we performed RNA-Seq to elucidate the difference in cellular signaling mechanisms between the two targets. Our previous study on cytoplasmic irradiation suggested that early responses such as mitochondrial fission were initiated 30 min postirradiation (*2*). Hence we chose early time points including 1 and 2 h postirradiation to screen for RNAs using RNA-Seq. GO analysis of biological process was performed using the genes significantly changed from cytoplasmic or nuclear irradiated samples, and the top 10 biological processes were listed in Table 3. Even though glucose metabolism was not on the top 10 list, many of the key enzymes involved in glycolytic pathways were significantly increased, including glucose transporter (GLUT3) in glucose transportation, PGC-1α in mitochondrial biogenesis and Pim-1 kinase (Fig. 1A). Pim-1, a kinase reported to increase PGC-1α expression and regulate glycolysis (*23*), was increased by threefold only in cytoplasmic irradiated samples. QPCR was used to further confirm the induction of glycolysis genes (Fig. 1B). Interestingly, the increased expression level of these key genes was seen 2 h postirradiation and sustained until 24 h or even 48 h postirradiation. On the contrary, targeted nuclear irradiation showed increase of genes in DNA-repair responses with little change in glycolytic genes (data not shown).

Rapid and Sustained Upregulation of Glycolysis Induced by Cytoplasmic Irradiation

To test if the increase in RNA level of glycolytic enzymes was indeed correlated with increased glucose flux, we performed 2-NBDG glucose uptake assay. Twenty-four hours after cytoplasmic irradiation, there was a significant increase in glucose uptake, indicated by increased fluorescence labelled 2-NBDG in SAE cells (Fig. 2A). Similar results were found in SAE cells 2 weeks postirradiation (Fig. 2B; CI). A significant increase of glucose uptake was observed in the cytoplasmic irradiated cells relative to control, $P \leq 0.001$. However, no increase of fluorescence intensity was found in nuclear irradiated cells (Fig. 2B; NI). Flow cytometry analysis further confirmed the increased glucose uptake as shown in Fig. 2C, 61% increase in fluorescence intensity was found in cytoplasmic irradiated SAE cells 2 weeks postirradiation while only minimal increase was seen in nuclear irradiated cells.

Consistent with the increase of glucose influx, an increase of lactate production was also found in cytoplasmic irradiated SAE cells (Fig, 2D). At 24 h postirradiation, a 39% increase in lactate production was detected in conditional medium harvested from cytoplasmic irradiated SAE cells relative to nonirradiated controls. This increase was maintained even up to 2 weeks postirradiation with a 43% increase in lactate production relative to controls. A slight increase of lactate concentration was found at 24 h after nuclear irradiation, however, this increase was transient as no further change was observed 2 weeks postirradiation (Fig. 1C), which was consistent with previously published data on irradiated tumor cells (*31*).

TABLE 3
GO Biological Process

ID	Name	Source	*P* value (CI)	*P* value (NI)
1	GO:0071396	Cellular response to lipid	1.69E-16	2.32E-08
2	GO:0033993	Response to lipid	4.51E-15	1.37E-10
3	GO:1901701	Cellular response to oxygen-containing compound	1.06E-12	NS
4	GO:0010941	Regulation of cell death	1.46E-12	2.37E-10
5	GO:0051254	Positive regulation of RNA metabolic process	2.81E-12	NS
6	GO:0006915	Apoptotic process	3.95E-12	1.85E-11
7	GO:0042981	Regulation of apoptotic process	4.76E-12	1.69E-10
8	GO:0012501	Programmed cell death	6.10E-12	2.78E-11
9	GO:0043066	Negative regulation of apoptotic process	6.37E-12	1.07E-07
10	GO:0043067	Regulation of programmed cell death	6.38E-12	2.19E-10

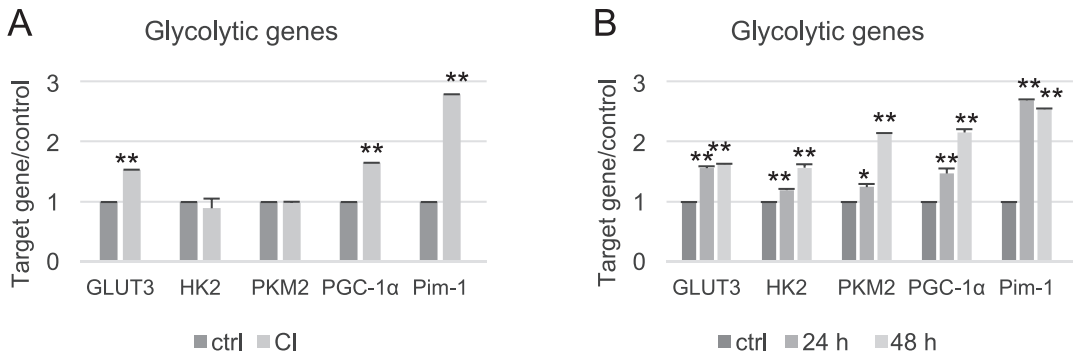

FIG. 1. Increased RNA level of glycolytic genes after cytoplasmic irradiation. Panel A: RNA-Seq (2 h) showed increase of glycolytic genes. RNA were collected from SAE cells and pooled from 50 individually irradiated microbeam dishes. RNA-Seq was performed Columbia University Genome Center and data was analyzed using the R program. Panel B: QPCR results confirmed increased RNA level of glycolytic genes. RNA were harvested 24 and 48 h postirradiation. RNA was extracted using Trizol. RT-QPCR was performed to confirm the expression level of glycolytic genes. β-Actin was used as reference gene. Error bar ± S.D.

Glycolysis Induction was Independent of Hif-1α

The upregulation or stabilization of Hif-1α have been reported to be the casual link between glycolysis and ionizing radiation (*26*). We next tested the potential role of Hif-1α in regulating cytoplasmic irradiation-induced glycolysis. To our surprise, in both RNA-Seq and immunofluorescence staining of cytoplasmic irradiated SAE cells, we did not observe a significant increase of Hif-1α (Fig. 3A and B; CI). Interestingly, distinct from cytoplasmic irradiation, we found significant upregulation in both RNA and protein level of Hif-1α after nuclear irradiation (Fig. 3A and B; NI; $P \leq 0.01$). Furthermore, application of Hif-1α inhibitor was not able to affect the level of lactate production induced by cytoplasmic irradiation (Fig. 3C). On the other hand, the slight increase of lactate production by nuclear irradiation [Figs. 2D (24 h) and 3C] was abolished by the presence of Hif-1α inhibitor suggesting the role of Hif-1α in mediating the subtle metabolic change induced by nuclear irradiation. Our data indicated that glycolysis induced by cytoplasmic irradiation was independent of Hif-1α.

Increase of Pim-1 Correlated with Increase of Glycolysis

Among all the genes that were regulated only by cytoplasmic but not nuclear irradiation, we identified the proto-oncogene serine/threonine-protein kinase (Pim-1) as a regulator of glycolysis. As shown in Fig. 4A and consistent with RNA-Seq results, there was an increased Pim-1 protein expression level after cytoplasmic irradiation. Small pharmaceutical inhibitor, Smi-4a have been generated to test the function of Pim-1 as an oncogene (*32*) and was used in this study. The presence of Smi-4a (5 μ*M*) completely abolished the increased glucose uptake 24 h postirradiation (Fig. 4B). No significant difference in glucose uptake was observed in nuclear irradiated cells. Consistent with the 2-NBDG glucose uptake assay, inhibition of Pim-1 using Smi-4a also significantly decreased the lactate production 24 h after cytoplasmic irradiation (Fig. 4C).

CRISPR/Cas9 was used to knockdown Pim-1 and further confirm the role of Pim-1 in cytoplasmic irradiation-induced metabolic shift. As shown in Fig. 5A, out of 6 gRNA sequences tested, gRNA no. 3 showed significant reduction of Pim-1 expression and was chosen to confirm the function of Pim-1. Figure 5B and C confirmed that with a more than 50% knockdown of Pim-1, the glucose uptake and lactate production was reduced by 96% and 55%, respectively. This data confirmed the importance of Pim-1 in regulating cytoplasmic irradiation induced glycolysis.

Pim-1 Inhibited AMPK to Mediate Glycolysis

Pim-1 has been reported to mediate energy metabolism by regulating AMP-Activated Protein Kinase (AMPK) activity (*23*), therefore, we tested the role of Pim-1 in regulating AMPK activity. Figure 5A shows the knockdown of Pim-1 by CRISPR/Cas9 system increased p-AMPK level by more than twofold. As shown below, using Pim-1 inhibitor also showed similar results. Both cytoplasmic and nuclear irradiation increased AMPK phosphorylation, suggesting an activation of AMPK (Fig. 6A). In combination of Smi-4a, a small molecule inhibitor of Pim-1, and cytoplasmic irradiation, there was a further increase of AMPK phosphorylation in SAE cells at 4 h postirradiation. Interestingly, increment of AMPK phosphorylation by Smi-4a was found in cytoplasmic irradiated SAE cells but not in nuclear irradiated cells, suggesting increase of AMPK activity by nuclear irradiation was independent of Pim-1.

Our previous results suggested a unique role of mitochondrial fission induced by cytoplasmic irradiation in mediating cellular responses including autophagy and apoptosis (*33*), therefore we tested the potential involvement of mitochondrial fission in regulating glycolysis. By inhibiting cytoplasmic irradiation induced mitochondrial fission using pharmaceutic inhibitor mdivi-1, we observed strong suppression of cytoplasmic irradiation induced Pim-1

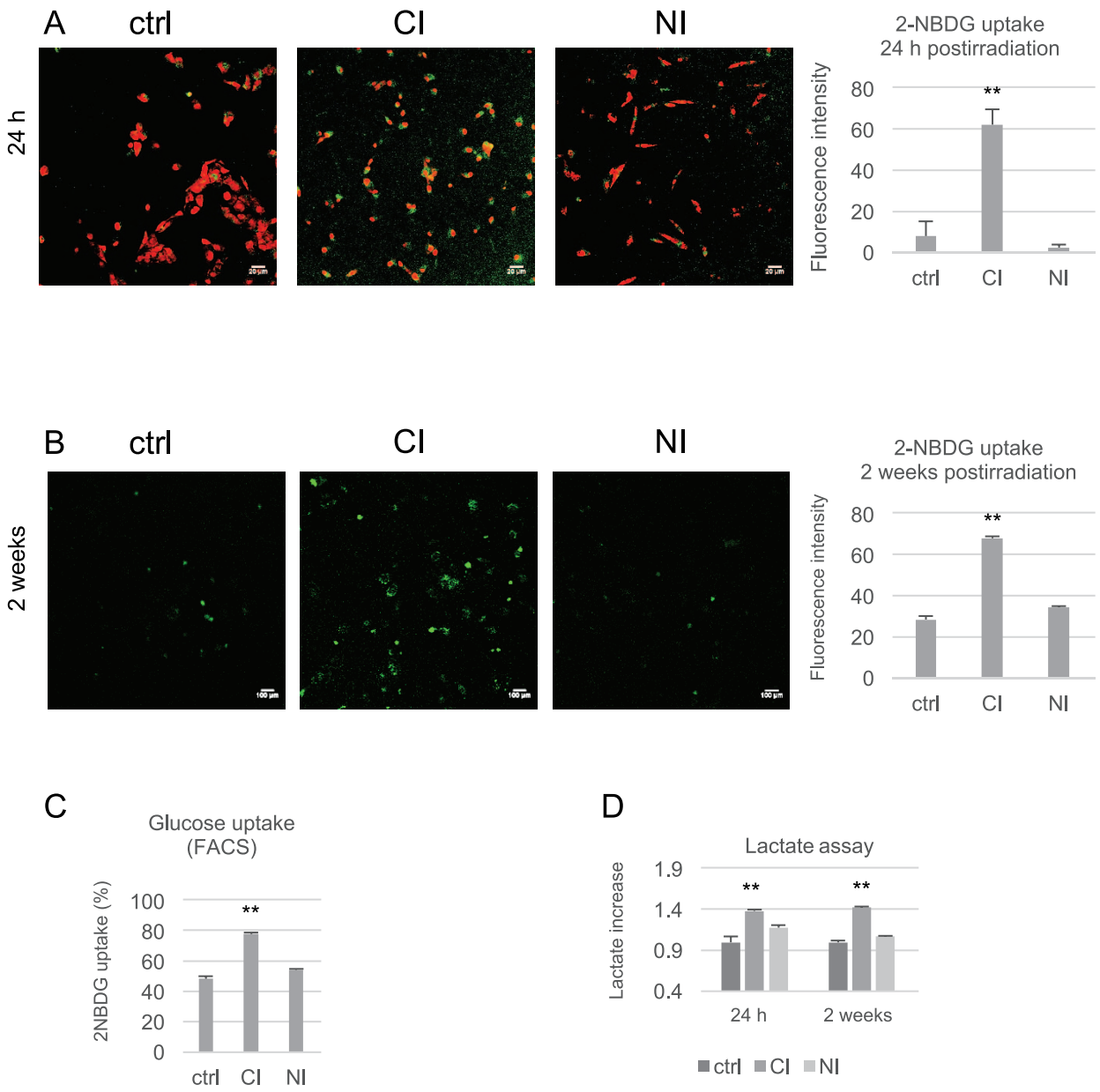

FIG. 2. Cytoplasmic irradiation increased glucose uptake and lactate production. Panels A and B: Increase of glucose uptake after cytoplasmic irradiation. Panel A: SAE cells were targeted irradiated either through cytoplasm (CI) or nucleus (NI) and incubated for 24 h. 2-NBDG (50 μ*M*) was added 1 h before fixation (green). Propidium iodide (PI, 20 μg/ml) was added to visualize nuclei (red). Fluorescence intensity was measured using ImageJ. Scale bar = 20 μm. Panel B: SAE cells were irradiated through cytoplasm or nucleus. Cells were trypsinized and pooled from 3 dishes for each treatment and incubated for 2 weeks. 2-NBDG (50 μ*M*) was added 1 h before fixation (green). Fluorescence intensity was measured using ImageJ. Scale bar = 100 μm. Panel C: SAE cells were incubated with 2-NBDG for 1 h before harvested for FACS. Fluorescence positive cell ratio was calculated based on total cell events. Panel D: Cytoplasmic irradiation increases lactate production. Conditional media were harvested from cells at indicated time (24 h or 2 weeks). Lactate concentration were measured and normalized to cell number. Lactate increase was calculated by comparing to the control (sham) irradiated sample. Error bar ± SD. $^{**}P < 0.01$.

expression (Fig. 6B). Consistent with the inhibitory effect on Pim-1 expression, mdivi-1 also significantly inhibited the lactate production after cytoplasmic irradiation (Fig. 6C; CI). We also tested the lactate production after nuclear irradiation with mdivi-1, our results showed no difference in lactate levels with inhibition of mitochondrial fission (Fig. 6C; NI) suggesting a selective inhibition of mdivi-1 on cytoplasmic irradiation induced glycolysis.

DISCUSSION

In the present study, we used RNA-Seq to explore the dynamic mRNA expression changes triggered by targeted subcellular irradiation. As described, different gene expression profiles were obtained in cytoplasmic or nuclear irradiated SAE cells. We reported herein that cytoplasmic irradiation led to rapid and sustained activation of glycolytic enzymes (Fig. 1). The upregulation of glycolytic enzymes

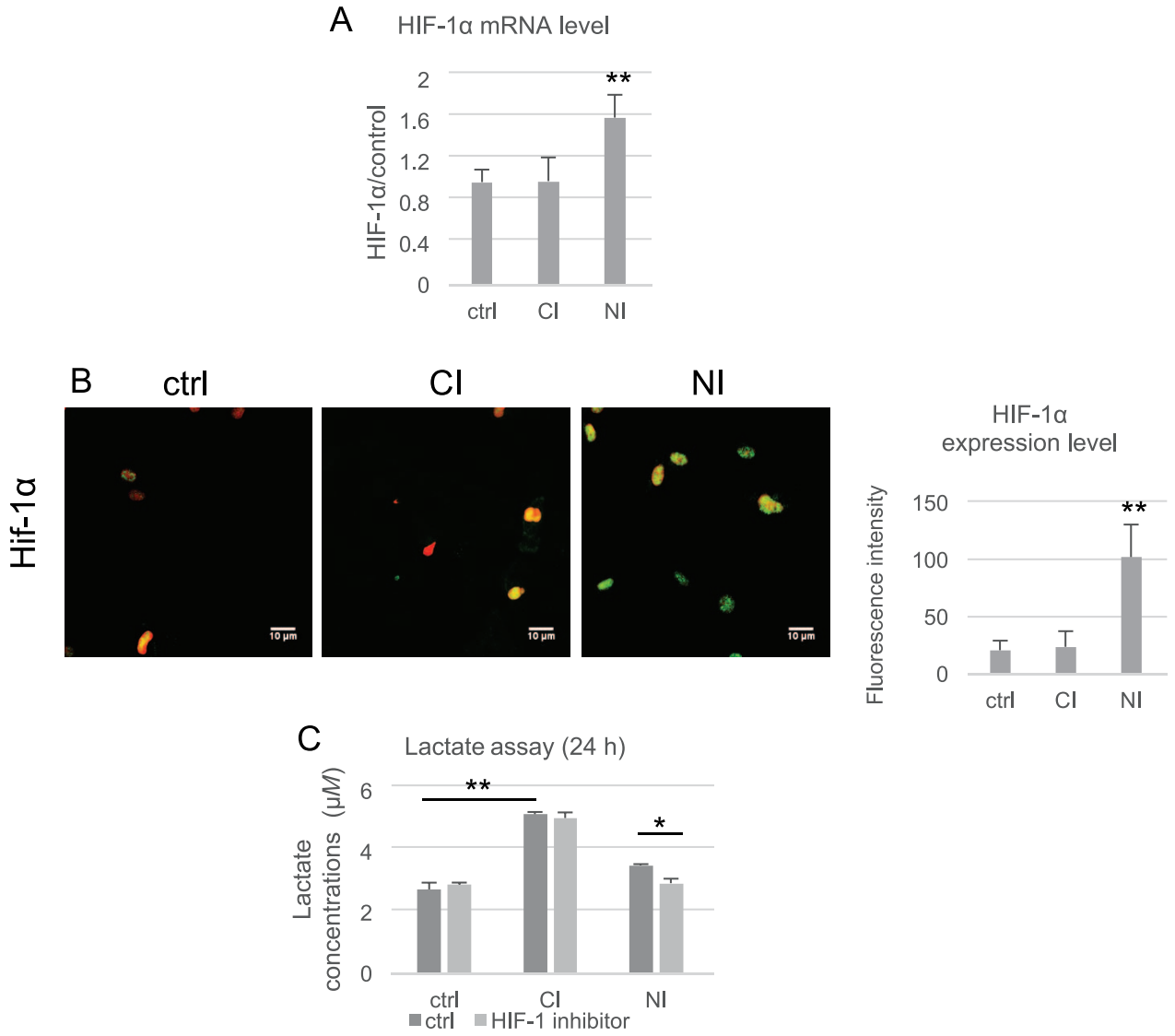

FIG. 3. Cytoplasmic irradiation induced glycolysis is independent of Hif-1α. A. RNA-Seq results of Hif-1α mRNA expression. RNA were harvested from SAE cells 2 h postirradiation. RNA-Seq was performed as shown in Fig. 1. Panel B: Hif-1α protein expression in SAE cells. Four hours after cytoplasmic or nuclear irradiation, SAE cells were fixed and immunofluorescence staining was performed. Hif-1α protein was visualized with Alexa Fluor 488 (green), nuclei were visualized using PI (red). Fluorescence intensity was quantified using ImageJ. Panel C: Hif-1α inhibitor has no effect on cytoplasmic irradiation induced lactate production. SAE cells were treated with Hif-1α inhibitor (50 μ*M*) for 30 min before irradiation. Hif-1α inhibitor was added back to culture media after irradiation. Conditional media were collected 24 h postirradiation and lactate concentration was measured using L-lactate detection kit. Scale bar = 10 μm. Error bar ± SD. $^{**}P < 0.01$.

led to extended increase in cellular glucose uptake and lactate secretion (Fig. 2). Furthermore, we confirmed the proto-oncogene serine/threonine kinase Pim-1 function as a regulator in the metabolic shift (Fig. 4). Although Pim-1 has been reported to drive glycolysis in cancer cells (*34*), to the best of our knowledge, our study is the first to report that Pim-1 functions independently of Hif-1α in mediating glycolysis in normal cells. We showed that Pim-1 inhibits AMPK activity to modulate glycolysis (Fig. 6A). Our data suggested that cytoplasmic irradiation and the subsequent mitochondrial stress that modified cell metabolic phenotype may contribute to the neoplastic conversion of normal cells under such environmental stress.

Due to the nature of attached cells on culture dish, it is evitable that targeted nuclear irradiation will involve traversal of cytoplasm. However, compared with nuclear irradiation, targeted cytoplasmic irradiation is relatively innocuous and induces fourfold less mutations at equivalent particle traversals (*3*). In the present study, cytoplasmic irradiation induced an upregulation of Pim-1 and glucose uptake while nuclear irradiation had no or minimal effects. It is likely that the transient increase in glycolysis mediated by Hif-1α induced by nuclear irradiation overshadowed the Pim-1 mediated response. Alternatively, the SAE cells attached to microbeam dish coated with Cell-Tak were relatively flat, leaving less cytoplasmic space as potential target when irradiated through the nucleus.

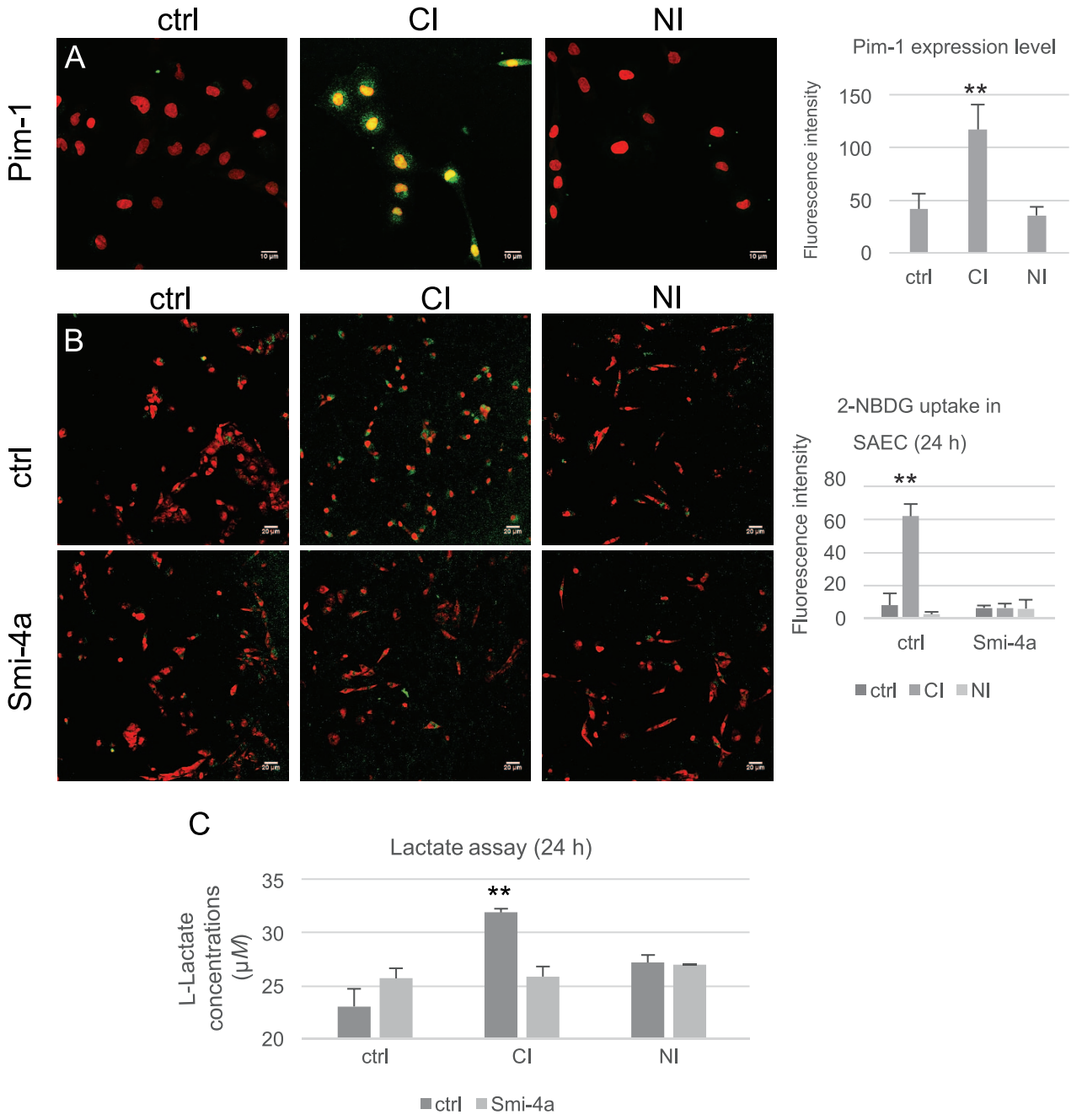

FIG. 4. Pim-1 regulates cytoplasmic irradiation induced glycolysis. Panel A: Pim-1 protein expression increased by cytoplasmic irradiation. SAE cells were irradiated at cytoplasm or nucleus and incubated for 24 h before fixation. Immunofluorescence was used to detect Pim-1 expression level (green). PI was used to visualize nucleus (red). Fluorescence intensity was quantified using ImageJ. Scale bar = 10 μm. Panel B: Pim-1 mediates cytoplasmic induced glucose uptake. SAE cells were treated with Smi-4a (5 μ*M*) or DMSO as control (ctrl, 0.1%) for 30 min before irradiation. 2-NBDG were added 1 h before fixation (green). PI was used to visualize nucleus (red). Fluorescence intensity was quantified using ImageJ. Scale bar = 20 μm. Panel C: Inhibition of Pim-1 suppressed cytoplasmic irradiation-induced lactate production. SAE cells were treated with Smi-4a (5 μ*M*) or DMSO as control for 30 min before irradiation. Smi-4a or DMSO were added back to culture media after irradiation. Conditional media were collected 24 h postirradiation and lactate concentration were measured using L-Lactate kit. Error bar ± SD. $^{**}P < 0.01$.

Due to the inherent limitation of a microbeam where individual cells are imaged and irradiated one at a time, only a limited number of cells can be irradiated at any one time. As a result, it is a major challenge to prepare high quality RNA samples for RNA-Seq. However, RNA-Seq has many advantages including accurate readout of transcriptomes, low background noise signal, large dynamic range of expression levels and more freedom over exploring new gene targets. In this study we chose early time points (1 and 2 h) to look for transcriptome changes. We observed differences in mRNA level of transcription factors, cytokine pathways, cell cycle regulator etc. which were consistent

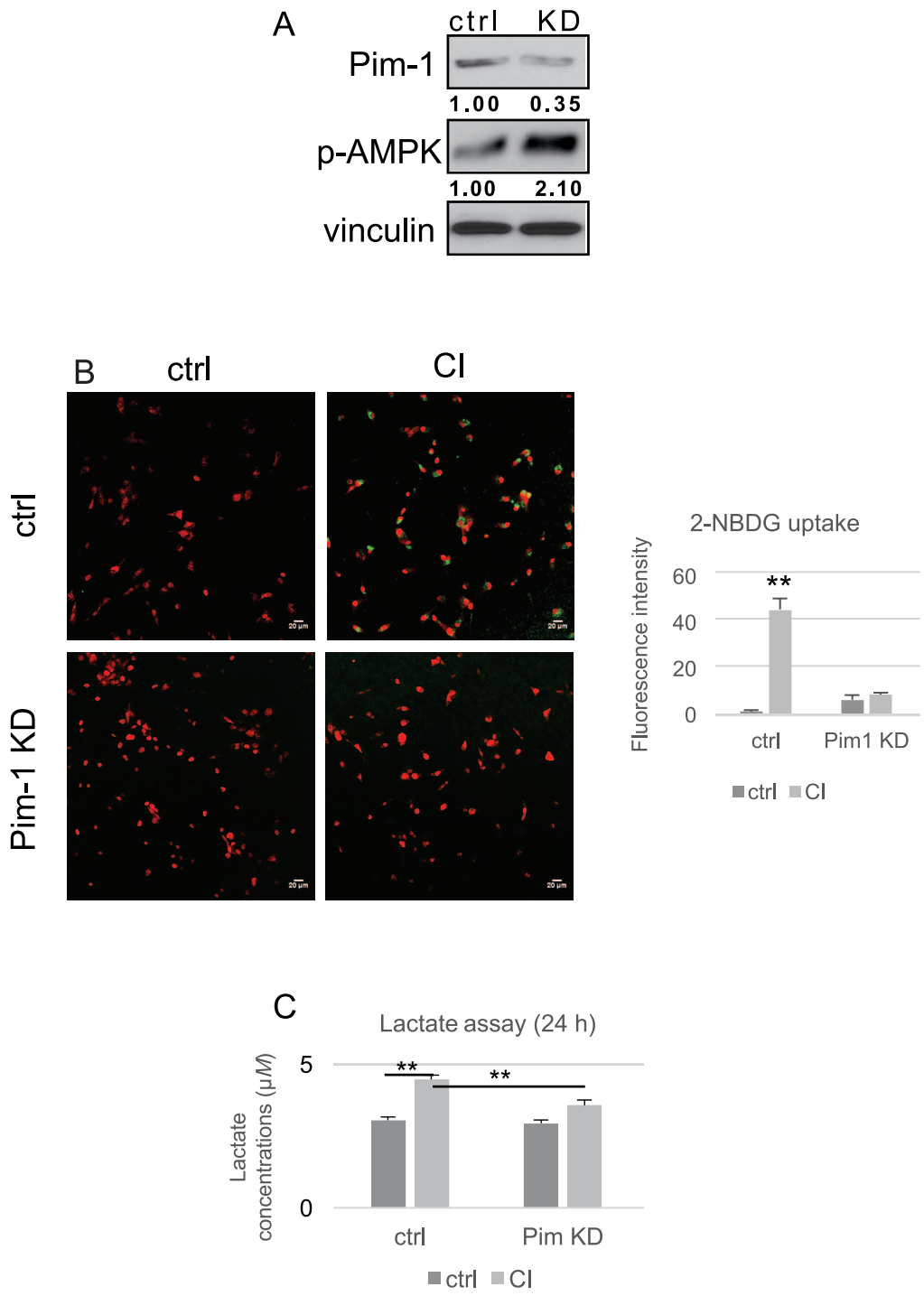

FIG. 5. Pim-1 knockdown confirmed important role of Pim-1 in regulating glycolysis. Panel A: Pim-1 knockdown (KD) showed increase level of p-AMPK. Pim-1 KD and control (ctrl) SAE cells were lysed for immunoblotting. Vinculin was used as loading control. Protein intensities were measured using ImageJ. Panel B: Pim-1 knockdown reduces glucose uptake. Control and Pim-1 knockdown SAE cells were cytoplasmic irradiated and incubated with 2-NBDG for 1 h before fixation. 2-NBDG was shown in green. Nuclei were visualized using PI (red). Scale bar = 20 μm. Fluorescence intensity was quantified using ImageJ. Panel C: Control and Pim-1 knockdown SAE cells were cytoplasmic irradiated and conditional media were collected 24 h postirradiation. Lactate concentration was determined using L-lactate kit. Error bar ± SD. $^{**}P < 0.01$.

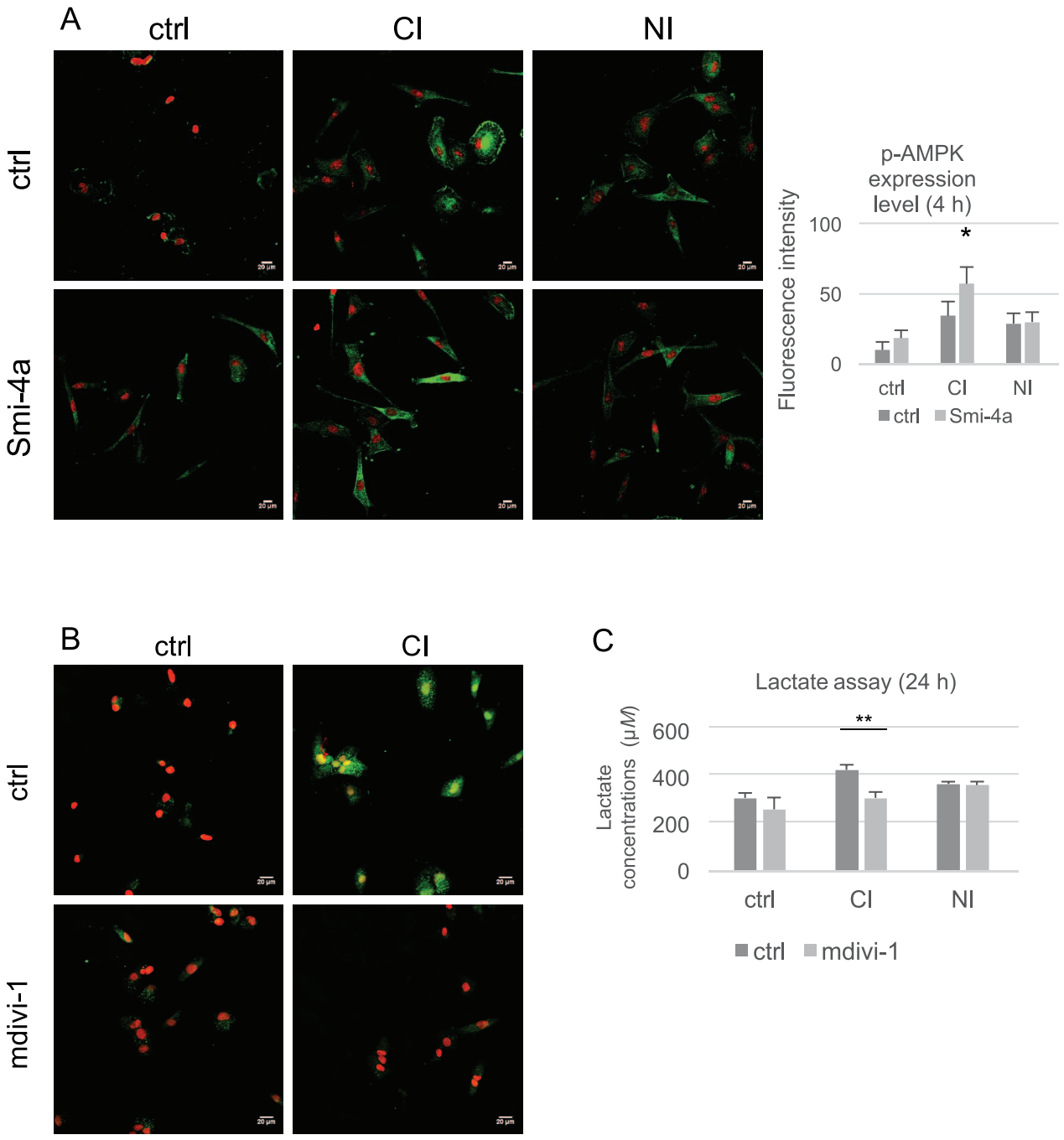

FIG. 6. Pim-1 inhibits AMPK to activate glycolysis. Panel A: Inhibition of Pim-1 by Smi-4a activated AMPK. SAE cells were treated with Smi-4a (5 μ*M*) 30 min before irradiation. Cells were fixed 30 min postirradiation and phosphor-AMPK were detected using immunofluorescence staining (green). Nuclei were visualized using PI (red). Fluorescence intensity was quantified with ImageJ. Scale bar = 20 μm. Error bar ± SD. *$P < 0.05$. Panel B: Mitochondria fission controlled Pim-1 upregulation. SAE cells were treated with mdivi-1 (50 μ*M*) for 30 min before irradiation. Cells were fixed for 4 h postirradiation. Immunofluorescence was used to detect Pim-1 (green). Nuclei were visualized using PI (red). Scale bar = 20 μm. Panel C: Mitochondria fission controlled lactate production. SAE cells were pre-treated with mdivi-1 (50 μ*M*) for 30 min. Conditional media were collected 24 h postirradiation and lactate concentration was determined using L-lactate kit. Error bar ± SD. **$P < 0.01$.

with our previous findings and provided interesting targets for future studies.

From the RNA-Seq results, we identified serine/threonine kinase Pim-1 to be the regulator for mediating glycolysis response to cytoplasmic irradiation. The mRNA level of Pim-1 was upregulated as early as 2 h after cytoplasmic irradiation and was maintained for weeks postirradiation (Fig. 1). Pim proteins have been reported to regulate mitochondria related protein expression including BAD (*35*) and PGC-1α (*23*). In cardiomyocytes, Pim-1 protein translocated into mitochondria in response to oxidative stress (*36*). Our results suggested the upregulation Pim-1 by

cytoplasmic irradiation was caused by mitochondrial fission (Fig. 6B), hence drew another link between Pim proteins and mitochondria function. However, how mitochondrial fission transcriptionally increase Pim-1 is not clear. Studies in vascular smooth muscle cells suggested transcriptional activation of Pim-1 requires signaling pathway of Janus-activated kinase (JAK), protein kinase C (PKC) and mitogen-activated protein kinase MEK1/2 (*37*). Other studies looked into multiple cancer cell lines and concluded Pim-1 expression was controlled by miR-33a (*38*). Further studies will be done to understand the signaling transduction between mitochondrial fission and transcriptional activation of Pim-1 and potential signaling feedback for the sustained activation of Pim-1.

Studies on Pim-1 and Pim family proteins suggested Pim proteins regulate glycolysis by regulating AKT (*34*), k-Ras (*39*) and PKM2 (*40*). In the current study, we also observed transcriptional upregulation of glycolysis mediators GLUT3, PKM2 and PGC-1α (Fig. 1). Interestingly, we noticed that knockdown of Pim-1 significantly reduced glucose uptake (Fig. 5B) but had less effect on lactate production (Fig. 5C). It is possible that glucose transporter 3 (GLUT3), one of the direct target of cytoplasmic irradiation (Table 3 and Fig. 1), may be regulated by Pim-1. Furthermore, other Pim family proteins may play redundant roles in regulating glycolysis after knockdown of Pim-1. Additionally, we found that Pim-1 had a negative regulation on AMPK phosphorylation/activation in promoting glycolysis (Fig. 6A). Toyama *et al*. concluded that AMPK could function as a sensor to monitor the energy status and promoted mitochondrial fission in bone osteosarcoma and mouse embryonic fibroblasts (*41*). In addition, Agnihotri *et al*. showed that increased ROS level in glioblastoma led to inhibition of PTEN-induced kinase 1 (PINK1) and mitochondrial dysfunction, which further activated glycolysis through upregulation of PKM2 (*42*). In our previous study, we reported a rapid mitochondrial fission 30 min after cytoplasmic irradiation which was gradually recovered after 12 h (*2*). Together these studies illustrated a general mechanism in both normal and tumor cell lines where mitochondrial fission mediated glycolytic shift. We have also observed kinetic change of AMPK phosphorylation status shortly after cytoplasmic irradiation (unpublished observation). Similarly, Kar *et al*. reported that in cardiomyocytes, oxidative stress induced by exposure to H_2O_2 led to phosphorylation of neuronal NOS through AMPK activity (*43*). However, further studies are required to elucidate the signaling cascade and interlink regulatory network between mitochondrial fission, PINK1, Pim-1 and AMPK.

This study was performed using high-LET alpha-particle radiation. Using the same charged particle microbeam, our previous study has shown that reactive radical species generated through membrane lipid peroxidation induces oxidative DNA damages and mutations in cytoplasmic irradiated cells (*1, 3*). Furthermore, treatment with the free radical scavenger, dimethyl sulfoxide (DMSO) and the lipid peroxidation inhibitor butylated hydroxyl toluene (BHT) could eliminate cytoplasmic irradiation-induced mitochondrial damage and other downstream effects (*1–3*). Compared with low-LET radiation, high-LET helium ions show enhanced numbers of long-range $^{\bullet}O_2^-$ and H_2O_2 (*44*) while low-LET ionizing radiation effect is dominated by short range $OH^{\bullet}$. Nonetheless, *in situ* generation of $OH^{\bullet}$ from $^{\bullet}O2^-$ and H_2O_2 contributed to their most cell-damaging effects (*45*). Hence, it is possible that cytoplasmic irradiation with low-LET radiation such as those generated using an X-ray microbeam may respond in a similar manner albeit at a reduced level.

In this study, we reported that high-LET cytoplasmic irradiation induced glycolysis in immortalized human SAE cells. Different from the minimal and transient glycolysis induced by nuclear irradiation through Hif-1α, cytoplasmic irradiation resulted in a sustained increase in glycolytic enzymes expression, glucose uptake and lactate production for at least two weeks. There is evidence that cytoplasm of basal and secretary cells among underground miners and home dwellers in high radon areas are threefold more likely to be traversed by an alpha particle than the nucleus (*46*). Our results provide a better understanding of the biological response of cells to low fluence of alpha-particle exposure and in radon-induced lung cancer. Finally, the identification of Pim-1 as the key regulator for radiation-induced glycolysis provides a novel target and the application of pharmaceutic inhibitors such as Smi-4a may prevent metabolic shift of normal tissue after radiation exposure.

ACKNOWLEDGMENTS

The authors thank members of the Radiological Research Accelerator Facility for their assistance with the microbeam irradiations (Drs. Guy Garty, Andrew Harkins, Alan Bigelow, Yanping Xu and Mr. Dennis Farrell) and to Dr. Fred Cheng-chia Wu for helpful discussion. This research was supported by the NIH grants 5P01-CA49062-23 and 5R01-ES12888-09. The Radiological Research Accelerator Facilities is an NIH sponsored Resource Center through grant EB-002033 (National Institute of Biomedical Imaging and Bioengineering). J. Wu is supported in part by the National Natural Science Fund of China 11305204.

Received: January 15, 2017; published online: February 7, 2017

REFERENCE

1. Hong M, Xu A, Zhou H, Wu L, Randers-Pehrson G, Santella RM, et al. Mechanism of genotoxicity induced by targeted cytoplasmic irradiation. Br J Cancer 2010; 103:1263–8.
2. Zhang B, Davidson MM, Zhou H, Wang C, Walker WF, Hei TK, Cytoplasmic irradiation results in mitochondrial dysfunction and DRP1-dependent mitochondrial fission. Cancer Res 2013; 73:6700–10.
3. Wu LJ, Randers-Pehrson G, Xu A, Waldren CA, Geard CR, Yu Z, et al. Targeted cytoplasmic irradiation with alpha particles induces mutations in mammalian cells. Proc Natl Acad Sci U S A 1999; 96:4959–64.
4. Hu B, Han W, Wu L, Feng H, Liu X, Zhang L, et al. In situ

visualization of DSBs to assess the extranuclear/extracellular effects induced by low-dose alpha-particle irradiation. Radiat Res 2005; 164:286–91.

5. Chen S, Zhao Y, Han W, Zhao G, Zhu L, Wang J, et al. Mitochondria-dependent signalling pathway are involved in the early process of radiation-induced bystander effects. Br J Cancer 2008; 98:1839–44.
6. Warburg O, On the origin of cancer cells. Science 1956; 123:309–14.
7. Vander Heiden MG, Cantley LC, Thompson CB, Understanding the Warburg effect: the metabolic requirements of cell proliferation. Science 2009; 324:1029–33.
8. Cairns RA, Harris IS, Mak TW, Regulation of cancer cell metabolism. Nat Rev Cancer 2011; 11:85–95.
9. Bensaad K, Tsuruta A, Selak MA, Vidal MN, Nakano K, Bartrons R, et al. TIGAR, a p53-inducible regulator of glycolysis and apoptosis. Cell 2006; 126:107–20.
10. Elstrom RL, Bauer DE, Buzzai M, Karnauskas R, Harris MH, Plas DR, et al. Akt stimulates aerobic glycolysis in cancer cells. Cancer Res 2004; 64:3892–9.
11. Brandon M, Baldi P, Wallace DC, Mitochondrial mutations in cancer. Oncogene 2006; 25:4647–62.
12. van Lohuizen M, Verbeek S, Krimpenfort P, Domen J, Saris C, Radaszkiewicz T, et al. Predisposition to lymphomagenesis in pim-1 transgenic mice: cooperation with c-myc and N-myc in murine leukemia virus-induced tumors. Cell 1989; 56:673–82.
13. Yuan LL, Green AS, Bertoli S, Grimal F, Mansat-De Mas V, Dozier C, et al. Pim kinases phosphorylate Chk1 and regulate its functions in acute myeloid leukemia. Leukemia 2014; 28:293–301.
14. Dhanasekaran SM, Barrette TR, Ghosh D, Shah R, Varambally S, Kurachi K, et al. Delineation of prognostic biomarkers in prostate cancer. Nature 2001; 412:822–6.
15. Warnecke-Eberz U, Bollschweiler E, Drebber U, Metzger R, Baldus SE, Holscher AH, et al. Prognostic impact of protein overexpression of the proto-oncogene PIM-1 in gastric cancer. Anticancer Res 2009; 29:4451–5.
16. Wang J, Kim J, Roh M, Franco OE, Hayward SW, Wills ML, et al. Pim1 kinase synergizes with c-MYC to induce advanced prostate carcinoma. Oncogene 2010; 29:2477–87.
17. Zippo A, De Robertis A, Serafini R, Oliviero S, PIM1-dependent phosphorylation of histone H3 at serine 10 is required for MYC-dependent transcriptional activation and oncogenic transformation. Nat Cell Biol 2007; 9:932–44.
18. Zhang Y, Wang Z, Li X, Magnuson NS, Pim kinase-dependent inhibition of c-Myc degradation. Oncogene 2008; 27:4809–19.
19. Bachmann M, Kosan C, Xing PX, Montenarh M, Hoffmann I, Moroy T, The oncogenic serine/threonine kinase Pim-1 directly phosphorylates and activates the G2/M specific phosphatase Cdc25C. Int J Biochem Cell Biol 2006; 38:430–43.
20. Morishita D, Katayama R, Sekimizu K, Tsuruo T, Fujita N, Pim kinases promote cell cycle progression by phosphorylating and down-regulating p27Kip1 at the transcriptional and posttranscriptional levels. Cancer Res 2008; 68:5076–85.
21. Li YY, Popivanova BK, Nagai Y, Ishikura H, Fujii C, Mukaida N, Pim-3, a proto-oncogene with serine/threonine kinase activity, is aberrantly expressed in human pancreatic cancer and phosphorylates bad to block bad-mediated apoptosis in human pancreatic cancer cell lines. Cancer Res 2006; 66:6741–7.
22. Zhang F, Beharry ZM, Harris TE, Lilly MB, Smith CD, Mahajan S, et al. PIM1 protein kinase regulates PRAS40 phosphorylation and mTOR activity in FDCP1 cells. Cancer Biol Ther 2009; 8:846–53.
23. Beharry Z, Mahajan S, Zemskova M, Lin YW, Tholanikunnel BG, Xia Z, et al. The Pim protein kinases regulate energy metabolism and cell growth. Proc Natl Acad Sci U S A 2011; 108, 528–33.
24. Shaw RJ, LKB1 and AMP-activated protein kinase control of mTOR signalling and growth. Acta Physiol (Oxf) 2009; 196:65–80.
25. Faubert B, Boily G, Izreig S, Griss T, Samborska B, Dong Z, et al. AMPK is a negative regulator of the Warburg effect and suppresses tumor growth in vivo. Cell Metab 2013; 17:113–24.
26. Zhong J, Rajaram N, Brizel DM, Frees AE, Ramanujam N, Batinic-Haberle I, et al. Radiation induces aerobic glycolysis through reactive oxygen species. Radiother Oncol 2013; 106:390–6.
27. Piao CQ, Liu L, Zhao YL, Balajee AS, Suzuki M, Hei TK, Immortalization of human small airway epithelial cells by ectopic expression of telomerase. Carcinogenesis 2005; 26:725–31.
28. Trapnell C, Pachter L, Salzberg SL, TopHat: discovering splice junctions with RNA-Seq. Bioinformatics 2009; 25:1105–11.
29. Trapnell C, Williams BA, Pertea G, Mortazavi A, Kwan G, van Baren MJ, et al. Transcript assembly and quantification by RNA-Seq reveals unannotated transcripts and isoform switching during cell differentiation. Nat Biotechnol 2010; 28:511–5.
30. Anders S, Huber W, Differential expression analysis for sequence count data. Genome Biol 2010; 11:R106.
31. Fujibayashi Y, Waki A, Sakahara H, Konishi J, Yonekura Y, Ishii Y, et al. Transient increase in glycolytic metabolism in cultured tumor cells immediately after exposure to ionizing radiation: from gene expression to deoxyglucose uptake. Radiat Res 1997; 147:729–34.
32. Lin YW, Beharry ZM, Hill EG, Song JH, Wang W, Xia Z, et al. A small molecule inhibitor of Pim protein kinases blocks the growth of precursor T-cell lymphoblastic leukemia/lymphoma. Blood 2010; 115:824–33.
33. Zhang C, Zhou H, Chao K, Hei T, Genotype-Dependent Tumor Inhibitory Effects of Metformin in Glioblastoma Cells. Int J Radiat Oncol Biol Phys 2014; 90:S798.
34. Leung CO, Wong CC, Fan DN, Kai AK, Tung EK, Xu IM, et al. PIM1 regulates glycolysis and promotes tumor progression in hepatocellular carcinoma. Oncotarget 2015; 6:10880–92.
35. Danial NN, Gramm CF, Scorrano L, Zhang CY, Krauss S, Ranger AM, et al. BAD and glucokinase reside in a mitochondrial complex that integrates glycolysis and apoptosis. Nature 2003; 424:952–6.
36. Borillo GA, Mason M, Quijada P, Volkers M, Cottage C, McGregor M, et al. Pim-1 kinase protects mitochondrial integrity in cardiomyocytes. Circ Res 2010; 106:1265–74.
37. Willert M, Augstein A, Poitz DM, Schmeisser A, Strasser RH, Braun-Dullaeus RC, Transcriptional regulation of Pim-1 kinase in vascular smooth muscle cells and its role for proliferation. Basic Res Cardiol 2010; 105:267–77.
38. Thomas M, Lange-Grunweller K, Weirauch U, Gutsch D, Aigner A, Grunweller A, et al. The proto-oncogene Pim-1 is a target of miR-33a. Oncogene 2012; 31:918–28.
39. Song JH, An N, Chatterjee S, Kistner-Griffin E, Mahajan S, Mehrotra S, et al. Deletion of Pim kinases elevates the cellular levels of reactive oxygen species and sensitizes to K-Ras-induced cell killing. Oncogene 2015; 34:3728–36.
40. Yu Z, Zhao X, Huang L, Zhang T, Yang F, Xie L, et al. Proviral insertion in murine lymphomas 2 (PIM2) oncogene phosphorylates pyruvate kinase M2 (PKM2) and promotes glycolysis in cancer cells. J Biol Chem 2013; 288:35406–16.
41. Toyama EQ, Herzig S, Courchet J, Lewis TL, Jr., Loson OC, Hellberg K, et al. Metabolism. AMP-activated protein kinase mediates mitochondrial fission in response to energy stress. Science 2016; 351:275–81.
42. Agnihotri S, Golbourn B, Huang X, Remke M, Younger S, Cairns RA, et al. PINK1 Is a Negative Regulator of Growth and the Warburg Effect in Glioblastoma. Cancer Res 2016; 76:4708–19.
43. Kar R, Kellogg DL, 3rd, Roman LJ, Oxidative stress induces phosphorylation of neuronal NOS in cardiomyocytes through

AMP-activated protein kinase (AMPK). Biochem Biophys Res Commun 2015; 459:393–7.

44. Azzam EI, Jay-Gerin JP, Pain D, Ionizing radiation-induced metabolic oxidative stress and prolonged cell injury. Cancer Lett 2012; 327:48–60.

45. Xu D, Liu D, Wang B, Chen C, Chen Z, Li D, et al. In Situ OH Generation from O2- and H2O2 Plays a Critical Role in Plasma-Induced Cell Death. PLoS One 2015; 10:e0128205.

46. Beir V, Health effects of exposure to radon. Committee on health risks of exposure to radon, Board on radiation effects research, Commission on life sciences, National Research Council 1999.